Role of particle gradation of clay-sand mixture on interfacial adhesion performance of polymer coating

Nidhi Murali[1], Jing Li[2], Anvi Agarwal[1], Patrick Berthault[2], Pijush Ghosh[1]

[1] Department of Applied Mechanics and Biomedical Engineering, Indian Institute of Technology Madras, Chennai, India

[2] Université Paris-Saclay, CEA, CNRS, NIMBE, 91191, Gif-sur-Yvette, France

Abstract

Interface performance between clay-sand mixtures and concrete structures are governed by the mixture composition and its physical properties. Moisture content and particle size distribution play a governing role in deciding the mixture fabric, its porosity, hydraulic conductivity, and its behaviour under various mechanical loading. Application of a polymer interfacial coating can improve the bond performance between soils and concrete mainly by interfacial friction/mechanical interlocking. The present work analyse the interfacial strength development between clay-sand mixtures and a polymer coating with changes in the particle gradation. The multi-scale mechanisms at the interface are investigated giving primary attention to soil porosity. A mixture of 50C:50S exhibited highest interfacial adhesive performance compared to other soil mixes. Also, moisture controlled pores and gradation controlled pores revealed difference in macroscale interfacial strength. Both Mercury Intrusion Porosimetry (MIP) and ^{129}Xe Nuclear Magnetic Resonance (NMR) were utilized to

This is a 'preproof' accepted article for Clay Minerals. This version may be subject to change during the production process.
DOI: 10.1180/clm.2024.7

detect the pore structure of the mixtures. ^{129}Xe NMR revealed the pore distribution of the mixture ranging from macropores to nanopores and MIP complemented the pore information by determining the critical pore entry diameter in the macropore regime. Mesopores dominated on increasing the fine sand content until a threshold value, thereafter merging of pores occurred and macropores dominated.

Keywords: Porosity, Mercury Intrusion Porosimetry (MIP), ^{129}Xenon NMR, Microstructure, Interfacial adhesion

1. Introduction

The formation of soil-structure interface guides the overall performance of the structural system. Predominantly for geotechnical works, cast-in-situ interface formation is widely preferred. In this, the cement grout is either directly cast or pressure grouted between compacted soil and structural material such as in pre-bored driven piles (Wang et al., 2020; Wu et al., 2023). Further, interface formation is affected by numerous parameters extending from macroscale features like asperities and undulations on surfaces to microscopic features like porosity, chemical interactions, surface energy, etc. The mechanical strength of an interface is affected by the surface roughness, surface texture and materials in contact (Alice et al., 2015; Pan et al., 2023). The shear behaviour of unsaturated soil-concrete interface is affected by matrix suction values. A lower water content favoured higher matrix suction and thereby higher interface shear performance (Chen & Liang, 2024). Conditioning of clay bricks for a period of 30 min increased the shear bond strength with mortar (Briceño et al., 2024). The importance of moisture content in driving the interface shear characteristics is explained in most of the above mentioned works.

Studies on interfacial behaviour between polymer coating and clay/cement substrates revealed adhesion mechanism at different length scales (Gujar et al., 2021, 2023; Ilango et

https://doi.org/10.1180/clm.2024.7 Published online by Cambridge University Press

al., 2021; Murali et al., 2022). Biopolymers, Cationic Polyacrylamide are widely used for soil stabilization applications and they have proved to be effective in freeze-thaw settings (Orts et al., 2007; Soltani-Jigheh et al., 2019). Hydrating cement surface exhibited a comparable adhesive strength (2-3 MPa) for epoxy coating at 2 days and 28 days of hydration whereas sodium bentonite clay exhibited interface adhesive strength in the range of 400-500 kPa. Epoxy aided in interface formation in each of the cases through different mechanisms. In case of clay, the diffusion of polymer into clay macropores at the surface coupled with hydrogen bond interaction between epoxy and oxygen donor sites on clay surface predominated. For cement, it was physical interaction between cement hydrates (C-S-H, CH) and epoxy groups that drives the interface formation. As understood from previous studies, pores in clay plays major role in interface formation. The nature of deposition and particle gradation give rise to inherent porosity in a clay. However, the porosity in clay can be affected by other environmental factors and also the proximity of the structural component. For example, the changes in porosity at the interface of cement and clay even at a distance of ~2 mm, due to dissolution and precipitation reaction within a barrier system was reported by Shafizadeh et al., (2020). Moreover, moisture content alters the soil porosity and this effect is predominantly seen for clayey soils (Feng et al., 2018). Hence, it is important to study the porosity variation in a clay-sand mixture and its contribution to interface formation with a polymer coating in the context of soil-structure interface.

A remarkable improvement in geotechnical properties of clay was achieved with the incorporation of lime-zeolite in it. Stabilization mechanism altered the microstructure of clay and contributed towards higher mechanical properties as explained in Khajeh et al., (2023). Any additive, be it conventional stabilizers or polymers enhance clay properties significantly at the macroscale by manipulating the pore microstructure in clay (Xia et al., 2023).

https://doi.org/10.1180/clm.2024.7 Published online by Cambridge University Press

Considering this aspect, the current study looks at the porosity effect on interfacial strength performance of polymer coated clay-sand mixtures.

Particular focus of this study is on clay-sand mixtures. Behaviour of clay-sand mixture under compressive loading is governed by the sand content. Effective load bearing capacity of these mixtures are guided by the threshold fine sand content, forming a sand skeleton within the matrix. However, addition of clay content may interfere with the hydraulic conductivity of the mixture (Tripathi & Viswanadham, 2012, Watabe et al., 2011). Clay-sand mixtures especially those present as sediments in estuaries, tidel inlets, etc. exhibit inter-fractional (sand-clay) interactions which guides their transport properties like deposition, erosion, etc (Cuthbertson et al., 2018). Our previous work explaining the microstructural mechanism of epoxy coated sodium bentonite revealed the formation of a diffused interface between epoxy and clay, primarily by epoxy percolation into clay surface pores (Murali et al., 2022). However, in real field conditions, profound variation in particle size of soil exists and this may drastically affect the porosity. To clearly understand the variation of soil porosity on the interfacial adhesive strength, different clay-sand compositions were considered.

A wide range of techniques such as cryo-SEM (Lubelli et al., 2013), MIP (Duan et al., 2013) are in practise to estimate the pore size distribution and pore connectivity of soil systems. However, conventional techniques pose a lot of challenges as most of them are destructive techniques. Usage of imaging techniques such as Scanning Electron Microscopy (SEM) to analyse the porosity changes in reinforced soil under drying-wetting cycles was reported by Hou et al., (2021) and use of FE-SEM to study porosity of gas/liquid plays of China were reported by Zhu et al., (2023). Various advanced NMR techniques were also used to understand the pore structure of soil, such as ^{1}H NMR relaxometry (Carrero-González et al., 2012), magnetic resonance imaging (MRI), ^{129}Xe NMR (Filimonova et al., 2011)(Tsiao et al., 1998).

https://doi.org/10.1180/clm.2024.7 Published online by Cambridge University Press

Both ^{1}H NMR relaxometry and MRI require a high water/solvent content, normally fully saturation inside samples for getting high signal-to-noise ratio, so they are not suitable for studying the soil samples with a small amount of water content. ^{129}Xe gas is a sensitive gas probe for NMR, which has been used to detect the pore structure regardless of the water content of various construction materials, such as cementitious materials, shales and geopolymers (Li et al., 2022). Hence, in this reported work, three soils at specific water content corresponding to their respective dry of optimum with different clay-to-sand ratios were prepared as schematically shown in Figure 1. ^{129}Xe NMR and conventional MIP methods were applied to provide complementary information of the porous structures of the three mixtures. The interfacial performance of each mix with a polymer coating was evaluated by analysing the shear load-displacement plot. The mechanisms were studied by taking into account the energy release rate expression put forward by Hölck et al., (2012). The evaluation of the effect of different porosities, obtained by varying the gradation of the soil, on the interfacial bond strength of epoxy coating is the specific objective of this work.

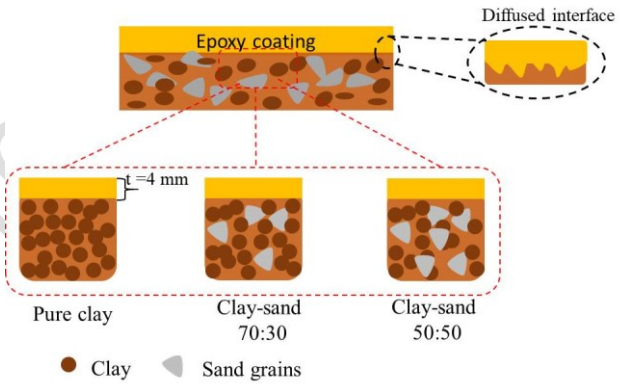

Figure 1. Schematic illustration of the epoxy coated clay-sand mixtures considered in the study. Different pore spaces found in a clay-sand mixture are evaluated by MIP and ^{129}Xe NMR

2. Materials and Methodology

https://doi.org/10.1180/clm.2024.7 Published online by Cambridge University Press

2.1 Materials

Soil: Soils considered were sodium bentonite (Na-Bt), a mixture of Na-Bt and fine sand in the proportions 70:30 and 50:50 by weight. The Optimum Moisture Content (OMC) and Maximum Dry Density (MDD) of all the mixes were calculated by performing Standard Proctor test as per IS 2720 part VII-1974 and are reported in Figure 2a. Pure bentonite exhibited the highest optimum moisture content of 34.96%. As sand content in mixture increases, the surface area of bentonite particles reduces for water absorption. Thus all clay-sand mixtures had lower OMC than pure Na-Bt (Agus et al., 2010). The particle size distributions of the mixes were evaluated by sieve analysis and that of Na-Bt by hydrometer analysis as per ASTM D7928-17. Particles of size 2 μm were predominant, with percentage finer of 80. These are shown in Figure 2b.

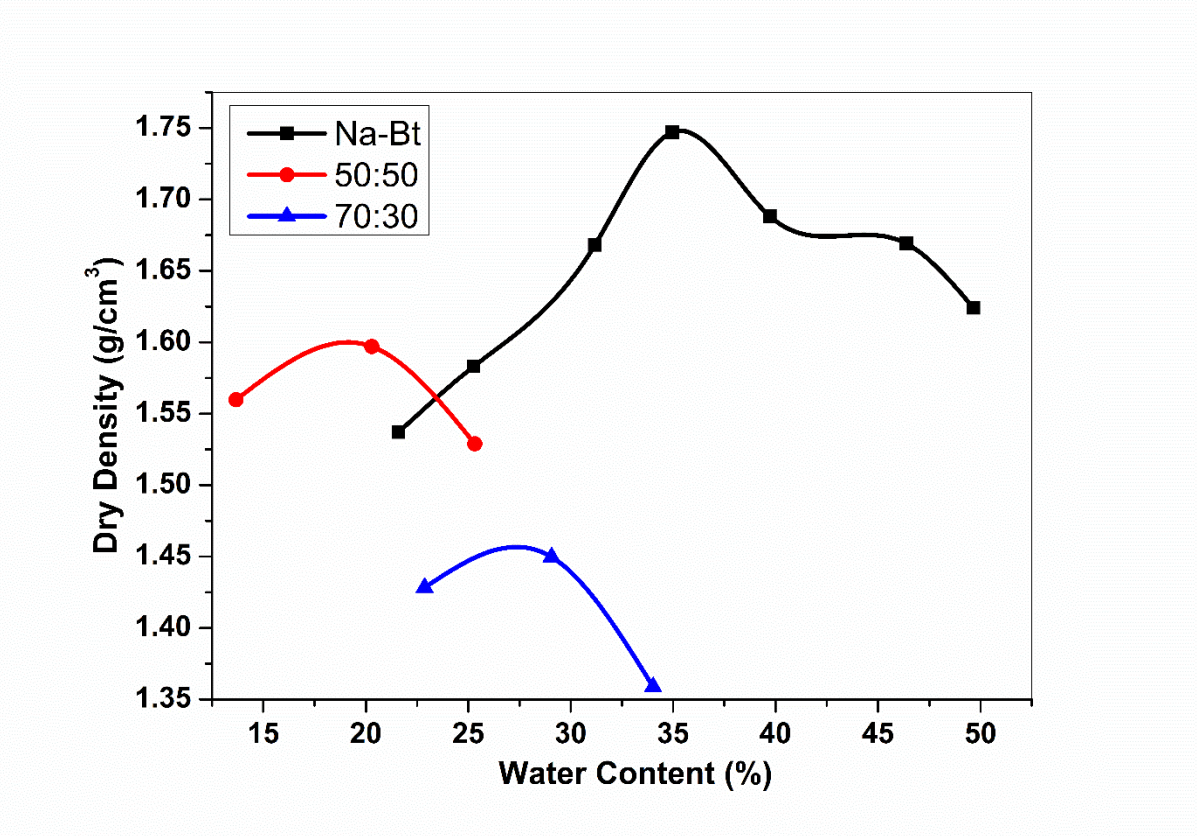

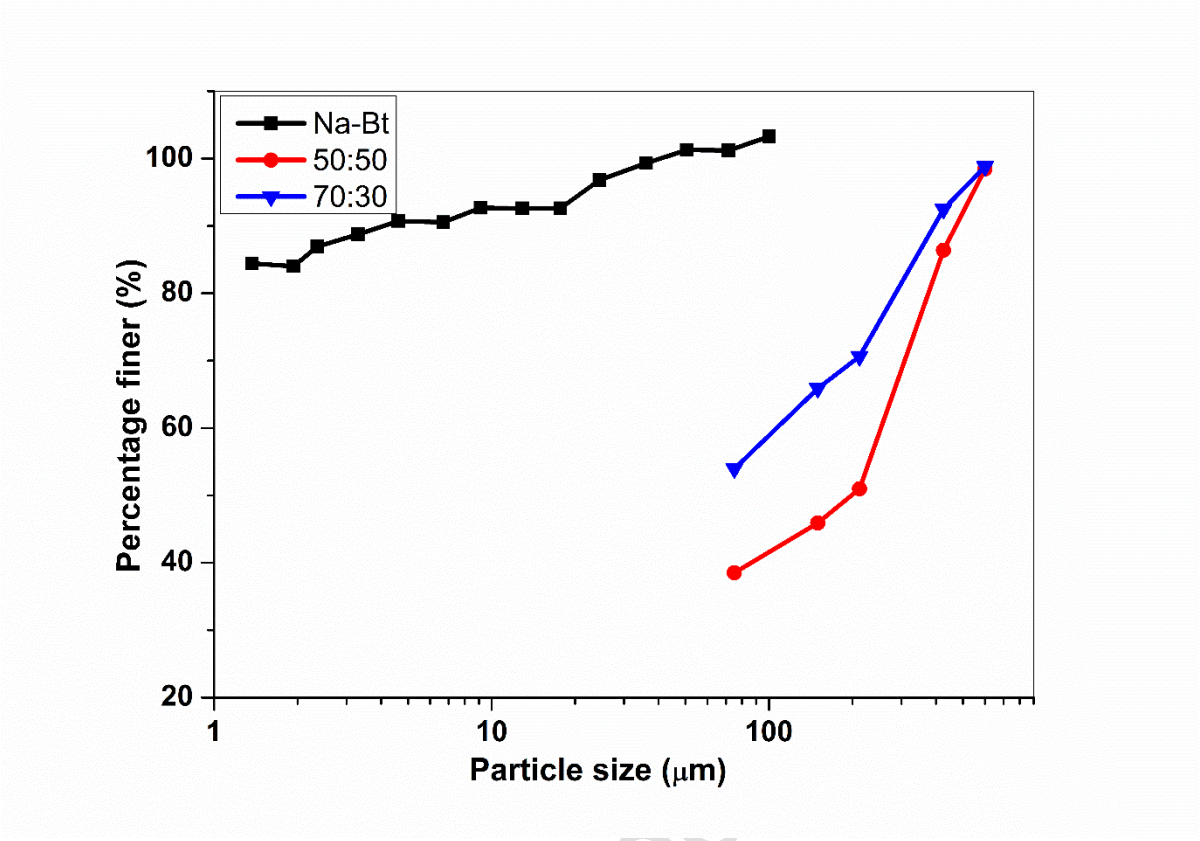

Figure 2 a) Proctor curves of all the mixes obtained as per IS 2720- Part VII- 1974.

b) Particle size distributions of clay-sand mixes.

Polymer: Bisphenol-A diglycidyl ether (DEGBA) resin and diethylene triamine (DETA) hardener were chosen as the polymer material for usage as a coating over compacted soil mass. The resin and hardener were used in the proportion 2:1 by weight and a curing period of 7 days at room temperature was provided.

2.2 Preparation of compacted clay-sand (C:S) mixtures

Each of the soil mixes were statically compacted in a square cutter of size 60 X 60 X 25 mm at bulk densities of 1.755 g/cm^3 and 1.773 g/cm^3 corresponding to the dry of optimum water content (i.e; OMC - 5%). One more sample of 60C:40S proportion having bulk density 1.718 g/cm^3 was also considered for NMR studies. Representative samples for porosity studies

https://doi.org/10.1180/clm.2024.7 Published online by Cambridge University Press

were collected from the compacted specimens and lyophilised to preserve the porosity. Lyophilised samples were stored in vacuum dessicators until they were tested.

For measuring the interfacial adhesion between compacted soil and epoxy coating, the samples were cast in shear box of size 60 X 60 X 10.5 mm. Two identical pieces were joined together maintaining a gap of 4 mm and epoxy resin was injected in between. The prepared sandwich composite samples were wrapped in cling film and kept in vaccum dessicator for 7 days to allow curing of the resin.

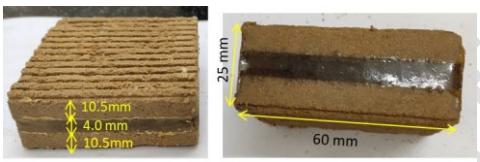

Figure 3 Clay-sand compositions coated with epoxy polymer prepared for shear testing. Curing of resin for 7 days was followed by testing in a conventional direct shear apparatus

2.3 Mercury Intrusion Porosimetry

Macropores and mesopores in the compacted soil masses were estimated by MIP. The instrument used was Pore master 60, Quantachrome, USA in the pressure range of 0.01 to 60000 psi. The pressure interval was 0.028 psi and data were recorded at a temperature of 23°C in order to lower the evaporation rate of mercury. MIP works on the principle that pressure at which mercury intrudes a pore is inversely proportional to its radius. This is mathematically represented by Washburn's equation as

$$\boldsymbol{P = \frac{-4\gamma \cos \theta}{d}} \qquad \text{Equation 1}$$

where,

P is the Pressure at which mercury intrudes in Pa ;

https://doi.org/10.1180/clm.2024.7 Published online by Cambridge University Press

ϒ is the surface tension of mercury ;

ɵ is the contact angle of mercury taken as 140º ;

d is the entry diameter of pore intruded in µm .

Samples prepared according to the methodology described in Section 2.2 were considered for MIP studies.

2.4 129Xe NMR on clay-sand composites

Xenon atom has large electron cloud, which makes Xe gas an ideal probe gas for NMR experiments because its NMR parameters are sensitive to the chemical composition and the physical structure of its environment. ^{129}Xe chemical shift reflects the pore size and structure, as the chemical shift (δ) of ^{129}Xe in the porous medium without strong adsorption sites can be modelled as the sum of three major contributions,

$$\boldsymbol{\delta = \delta_0 + \delta_{Xe-Xe} + \delta_{Xe-S}} \qquad \text{Equation 2}$$

where the δ_0 is the chemical shift of the ^{129}Xe gas at 0 pressure; $\delta_{Xe\text{-}Xe}$ is the interaction term, coming from collision of ^{129}Xe atoms, which can be neglected at low gas pressures. $\delta_{Xe\text{-}S}$ represents the collision between ^{129}Xe with the pore wall and it is therefore dependent on the pore size and the pore surface. Since the surface of the pore is constant in the same studied material, the change in δ is inversely proportional to the pore size.

Before performing the ^{129}Xe NMR experiment, the prepared three cylindrical clay:sand samples with diameter of 7.6 mm and height of 20 mm were put into three 8 mm diameter NMR glass tubes with screw caps, respectively. About 1.5 bar of ^{129}Xe gas was introduced into each tube by using a vacuum system. Xenon enriched at 83% in 129 isotope was purchased from Eurisotop (Saclay, France).

https://doi.org/10.1180/clm.2024.7 Published online by Cambridge University Press

The ^{129}Xe spectra were then recorded at room temperature on a narrow-bore 11.7 Tesla spectrometer (Bruker, Rheinstetten, Germany) equipped with an 8 mm micro-imaging probe. The experiments were performed by using one-pulse sequence, with pulse length of 13 μs at a power of 75 W. The spectra were accumulated with an interscan delay of 50 s. The chemical shift of the free Xe signal was calibrated to ^{129}Xe gas pressure/2, which is 1.5/2 = 0.75 ppm (Bonardet et al., 1999). The ^{129}Xe NMR spectra were fitted by using the program 'dmfit'. (https://nmr.cemhti.cnrs-orleans.fr/dmfit/). The spectra were decomposed to several Lorentzian lines.

2.5 Measurement of adhesive strength of epoxy-coated compacted clay:sand mixture

Rapid shear test was performed to evaluate the interfacial shear strength employing a conventional direct shear apparatus at a displacement rate of 1.25 mm/min under surcharge loads of 100 kPa, 200 kPa and 300 kPa. Failure was allowed to take place along the interface between epoxy and soil substrate. The interfacial shear strength (τ) was evaluated by the expression $\frac{P}{A}$ where, P is the load cell reading in kN ; and A is the initial cross-section area in m^2 .

3. Results and Discussions

According to Hölck et al., (2012), the critical energy release rate (G_c) when two adhesively bonded surfaces separate is represented by the expression

$$G_c = (w_{12} + w_{chem})(1+\phi) + \Delta h \qquad \text{Equation 3}$$

The terms, w_{12} and w_{chem} represents the physical and chemical bonded interactions between the bonded surfaces. In this study, these are the soil and epoxy surfaces. Contribution of w_{chem} is neglected as there are no suitable sites for chemical bond formation between the two. Physical interaction is attributed to hydrogen bonded interaction between epoxy functional

https://doi.org/10.1180/clm.2024.7 Published online by Cambridge University Press

sites and negatively charged oxygen sites on clay (Murali et al., 2022). The term (1+ϕ) refers to the surface area available in the form of accessible pore, surface undulations, etc. This aspect of interface formation is given attention through this study. Further, the heat dissipated at the time of debonding of two surfaces under study is denoted by Δh. The enhancement in surface area through pore size distribution has a direct correlation to the energy release rate. Each of the clay-sand mixture were prepared at a moisture content to the dry of optimum. Figure 4 depicts the specific dry of optimum moisture content for each of the mixes. There is a difference of 12.19% in moisture content between Na-Bt and 50:50 mixture. As there are changes in water content in each of these mixes, the net unbalanced forces on the surface of the compacted substrates of each of these mixes might also vary. According to Goebel et al., (2004), the contact angle and surface energy of soils depend on aggregate fraction and water potential. A key parameter affecting the contact angle and eventually surface energy in soils are water potential or moisture content. The surface free energies of aggregate and homogenised soil were in the range of 55 – 65 mJm^{-1}. Out of the two components, polar component showed variation (32 - 45 mJm^{-1}) with aggregate size whereas dispersive component remained similar. The difference in polar component is primarily due to two reasons. One is availability of clay electron donor locations on the soil surface acting as base component. Second is acid component of surface energy which are negligibly small in soils. In the soil mixtures considered, a variation in base component of surface energy is expected because both moisture content and aggregate fraction are varying. However, decoupling the individual contribution is not within the scope of this study. More focus is given to changes in surface porosity variation arising from particle gradation as explained in the next sections.

https://doi.org/10.1180/clm.2024.7 Published online by Cambridge University Press

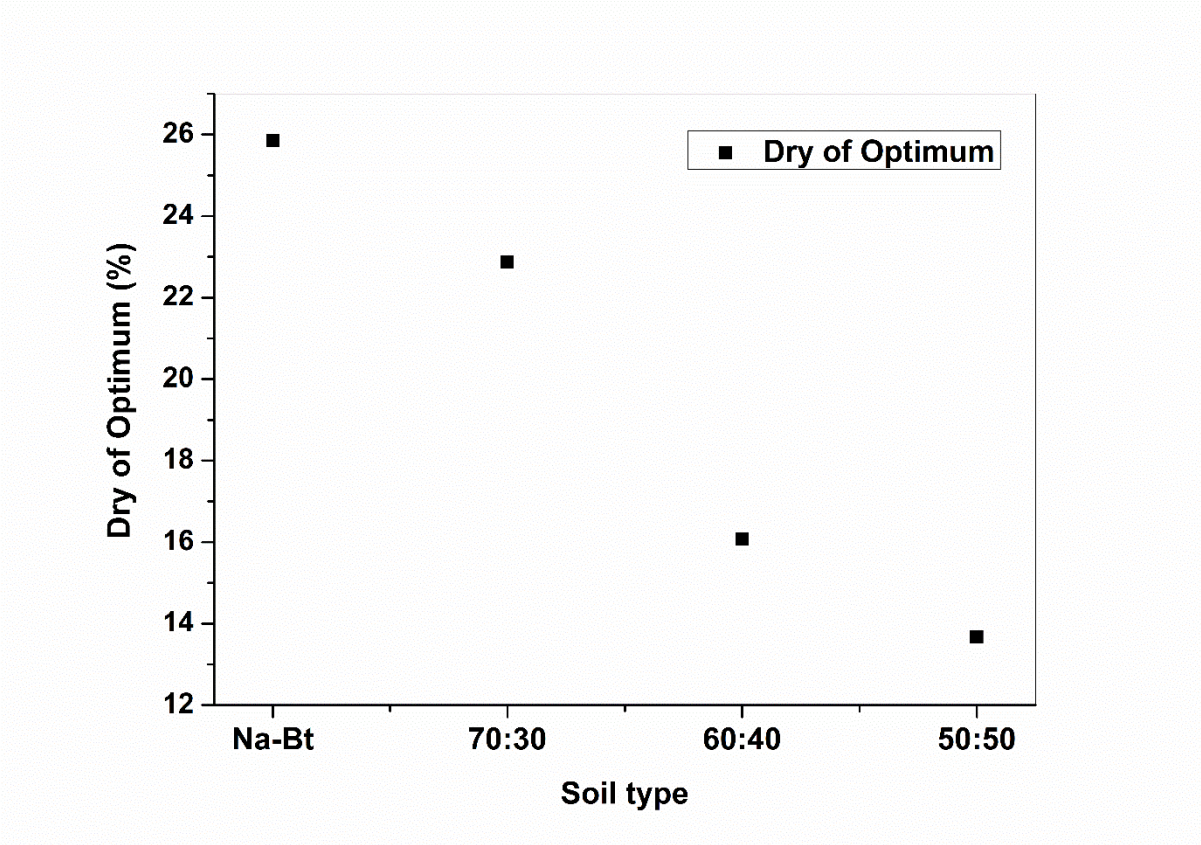

Figure 4 Moisture content at which soil substrates were prepared. 50:50 mix is at a water content 10% lesser than pure Na-Bt

3.1. ^{129}Xe NMR spectra of clay-sand mixes

The ^{129}Xe NMR experimental spectra and the fitted spectra of three samples are shown in Figure 5. The spectra of all three samples show a signal at 81 ppm. This is attributed to a small space, resulting from the ^{129}Xe gas adsorbed into the clay matrix, which was also found in pure clays (Tsiao et al., 1998). In addition, a peak at around 1 ppm is also observable for all samples. This is attributed to the fast exchange peak between the free ^{129}Xe gas with the ^{129}Xe gas in the macro-scaled space. The macro-scaled space corresponds to mainly the space between sand particles with size > 50 nm.

The signal in the middle of the spectrum is different for three samples. For the two samples of C50:S50 and C70:S30, it appears at 50 ppm and 29 ppm, respectively. A large signal is

https://doi.org/10.1180/clm.2024.7 Published online by Cambridge University Press

observed for the sample of C60:S40, and it is fitted to two Lorentzian lines. The fitted peak chemical shifts of the two compositions were centered close to the middle peaks in the other two samples, respectively (Table 1). These two fitted compositions at 40 and 30 ppm were assumed to be a small pore and a macro pore respectively.

For the mixture with the clay-to-sand ratio of 50:50, the peak at 1 ppm dominates, accounting for 74%. This is reasonable since the high sand content makes a large amount of macro-scaled space among sand particles, this mixture has larger averaged macroporous size than the other two mixtures. When more small clay particles were added to increase the clay-to-sand ratio to 60:40 and 70:30, the middle peak became the main peak with a proportion of over 71%. This is because more small clay particles filled in the space between large sand particles and the volume of macropores get filled up compared to a 50:50 mix.

The middle peak shifted to the larger chemical shift region, which is the smaller pore size region as the clay-to-sand ratio decreased from 70:30 to 50:50. At higher clay content, sand particles float within the matrix without any particle to particle contact, thus the major feature of such a mixture is the presence of mesopores and nanopores from clay aggregates and clay galleries.

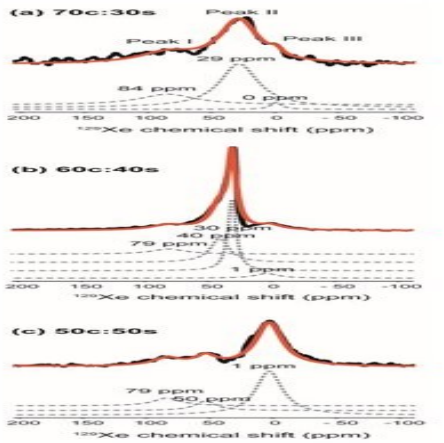

Figure 5 ^{129}Xe NMR spectra (black solid lines) and the fitted spectra (red solid lines) of (a) 70c:30s, (b) 60c:40s and (c) 50c:50s. The fitted components are plotted as dotted lines.

https://doi.org/10.1180/clm.2024.7 Published online by Cambridge University Press

Table 1 Distribution of porosity in all the mixes across the entire pore size regime

Clay:sand ratio		Peak I	Peak II		Peak III
			Component I	Component II	
70:30	Peak chemical shift (ppm)	84	-	29	1
	Integral percentage (%)	25.0	-	71.8	3.2
60:40	Peak chemical shift (ppm)	79	40	30	1
	Integral percentage (%)	13.1	34.5	44.3	8.1
50:50	Peak chemical shift (ppm)	79	50	-	1
	Integral percentage (%)	13.4	12.3	-	74.3

3.2. Pore size distribution by MIP

The information obtained from Xenon NMR spectra provided a qualitative idea of pore size distribution in clay-sand mix soil. Specific details such as critical pore diameter cannot be obtained from this technique. Information on exact pore entry diameter is essential to analyse the interfacial adhesive strength performance. To help us understand better about different pore size regimes, MIP technique was employed. The pore size distribution of all soil mixes were estimated by MIP and the differential intrusion plot obtained for all the soil mixtures are shown as in Figure 6. Mixture 60C:40S is excluded from the intrusion curve based on the findings from interface shear testing which are given in Section 3.3.

https://doi.org/10.1180/clm.2024.7 Published online by Cambridge University Press

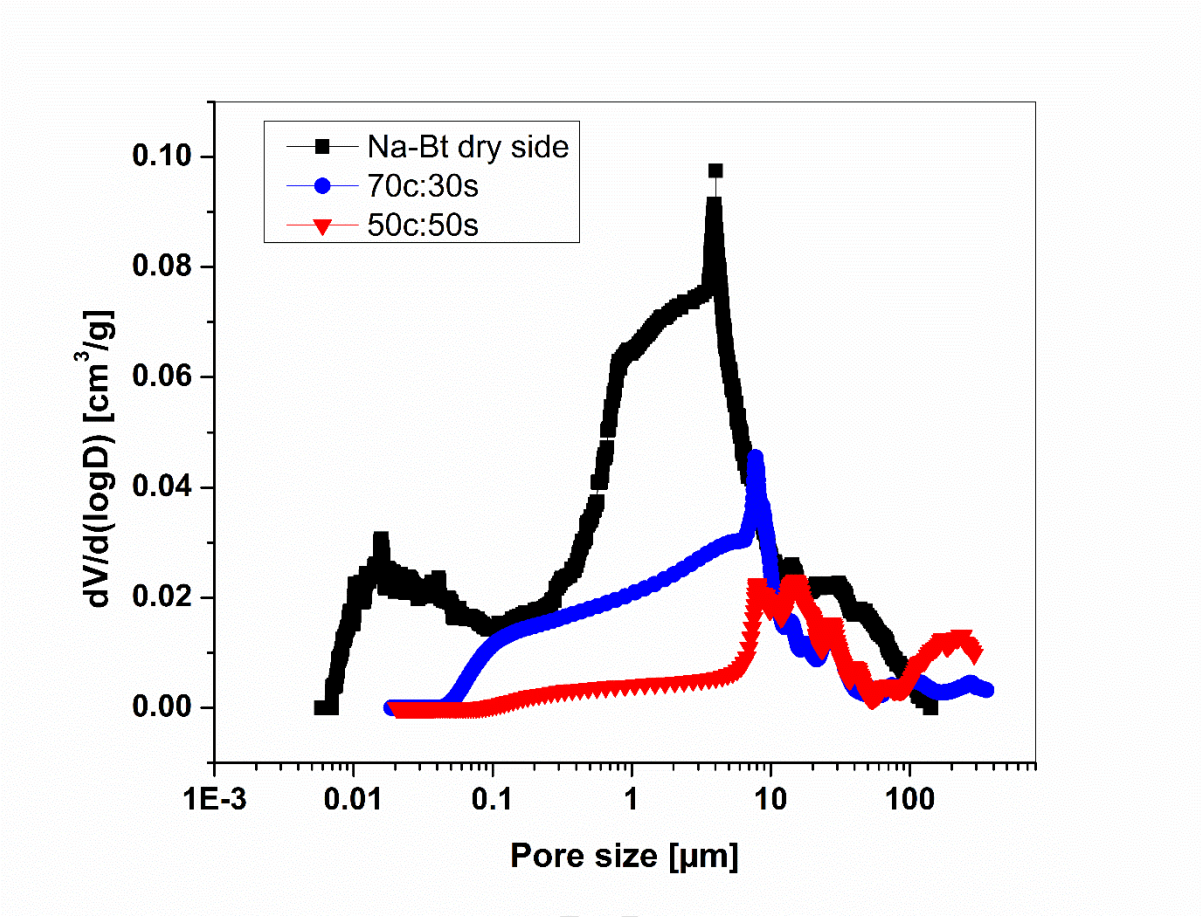

Figure 6 Differential Intrusion Plot of clay:sand mixtures showing the critical pore entry radius. Pure clay exhibits a higher macropore volume. Clay-sand mixes gradually shifts to unimodal distribution as sand content increases

Pure Na-Bt exhibits bimodal distribution, one each at macropore and at mesopore regime. The other soil mixes gradually shift from bimodal to unimodal distribution as the mix proportion was varied from 70:30 to 50:50. With equal fraction of clay and sand, we see a predominance of pores of 10 -12 µm in the macropore regime and near-to-zero mercury intrusion in the mesopore regime. The critical pore entry radius obtained for 50:50 mix is 11 µm with intrusion volume of 0.02 cm^3/g. As clay content goes down from 100% to 50%, the critical pore entry radius increases from 4 µm to 17 µm. The arrangement of sand within a matrix of clay takes place according to the percentage of clay content as depicted in (Figure 7 a-d). As a small fraction of clay gets replaced by sand, sand particles gets sparsely populated

https://doi.org/10.1180/clm.2024.7 Published online by Cambridge University Press

within clay matrix. Afterwards, when the clay fraction reduces, the intergranular space between sand particles becomes closer and less populated with clay (Figure 7 b). When the clay fraction further goes down, the sand particles attains inter-grain contact. At this stage, very few of the inter-granular sand voids are filled with very loosely packed clay as illustrated in Figure 7 d. For the formation of a partial skeleton of sand, an optimum replacement of clay fraction is required. This study deosn't focus on arriving at optimum fines content. However, the changes in porosity arising from the arrangement of different grains is considered as the mechanism behind changes in interfacial strength for different mixtures. This is reflected in the critical pore entry radius of 50:50 mix compared to a pure Na-Bt mix. Mix 50:50 was characterized by critical pore entry radius of 17 μm compared to 8.14 μm and 4 μm of 60:40 and 50:50 mixes. This behaviour occurs as small clay grains arrange in a more closely packed manner and reduces the macropore size. However, the very high intrusion volume (0.09 cc/g) by mercury in pure Na-Bt is interesting to note. Also, we did not arrive at the threshold fines content to obtain the highest inter-particle contact between sand as this may not have a positive impact on interfacial bond strength.

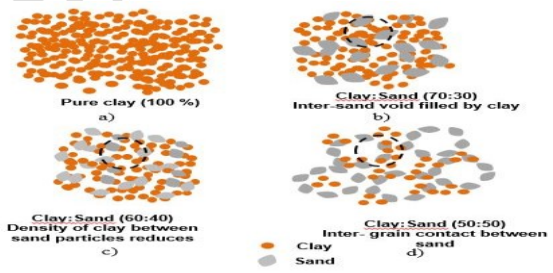

Figure 7 Schematic illustration of porosity variation in a clay:sand mixture a) pure clay b) 70C:30S Sand particles sparsely populated inside clay matrix c) 60C:40S Inter-sand space filled by loosely packed clay d) 50C:50S Inter-grain contact between sand leads to partial skeleton (Black dotted circle represents changes in inter-sand void as clay content reduces) (adapted from Vallejo et al. 2000)

https://doi.org/10.1180/clm.2024.7 Published online by Cambridge University Press

The lower particle size of clay grains give rise to smaller pores when clay proportion increases from 50% to 100%. Also, they exhibit a higher porosity compared to the larger, angular sand grains as seen by the higher intrusion volume. This particular behaviour of clay is attributed to its mineralogy and particle size (Horpibulsuk et al., 2010). For Na-Bt, there are two distinct peaks clearly demarcating the pore size regimes in macropore (> 50 nm) and mesopore (2-50 nm). Miller & Sower (1958) studied the strength characteristics of soil-aggregate mixes. The highest density was obtained at 26% fines and 74% aggregate content. As the fine content increases beyond a threshold value, the interparticle contact between sand grains reduces, this can give rise to higher cohesion and lower frictional value (Havens & Goodwin., 1951). Obtained values of porosity distribution in the clay-sand mixes agrees with the mechanism explained by Miller & Sowers, (1958).

3.3 Interfacial adhesive strength between epoxy coating and soil

The interfacial adhesion between all the soil mixes and epoxy coating were determined to understand the effect of porosity on the adhesion mechanism. Out of all the mixes, clay:sand at 50:50 exhibited the highest interfacial strength for all the normal stresses followed by Na-Bt and 70:30 respectively as depicted in Figure 8. The error bar of interfacial adhesive strength at each normal stress is given in Figure 9. The reasoning for this highest strength exhibited by 50:50 mix can be linked to the pore size distribution of the mixture. The macropore regime is more broader for 50:50 mix and is 74.3% in comparison to the much lower macropore porosities of 60:40 (8.12%) and 70:30 (3.21%). The highest interfacial strength of 450 kPa was observed at 300 kPa normal stress and is directly correlated to the formation of higher interface thickness (polymer penetration). However, Na-Bt exhibited a slightly higher interfacial adhesive strength at 300 kPa. This increase at higher normal stress is possibly due to increased shear contact area and the extended epoxy deformation occurring inside the pores. Actual epoxy coated specimens exhibit adhesive failure across the interface

https://doi.org/10.1180/clm.2024.7 Published online by Cambridge University Press

as shown in Figure 10. Here, as 50:50 mix exhibits a higher critical pore entry radius than pure Na-Bt, a higher intrusion by epoxy is possible and therefore a higher interface thickness.

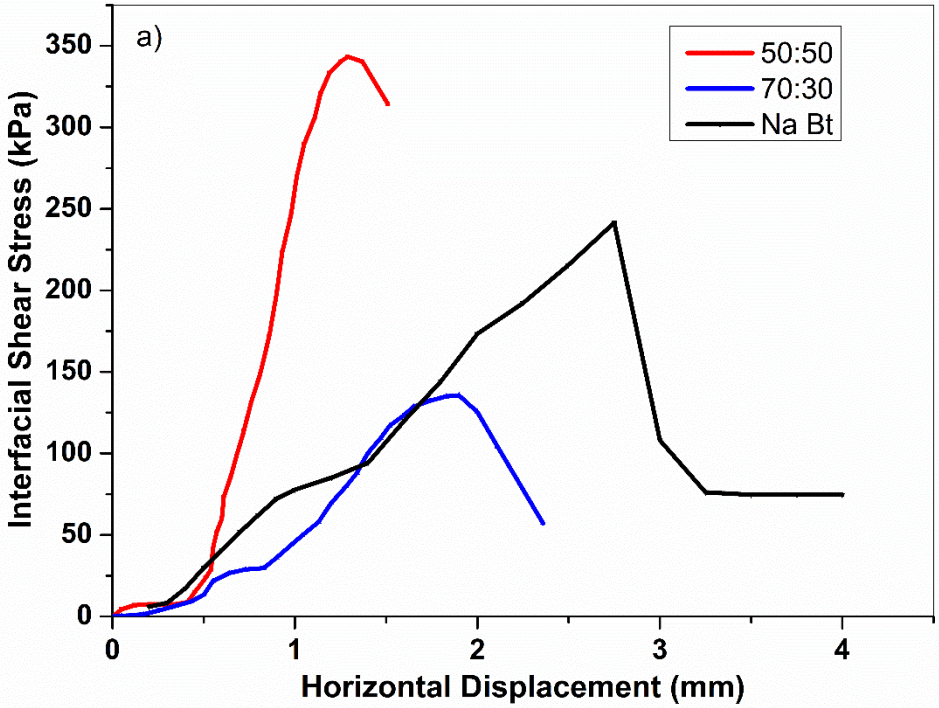

https://doi.org/10.1180/clm.2024.7 Published online by Cambridge University Press

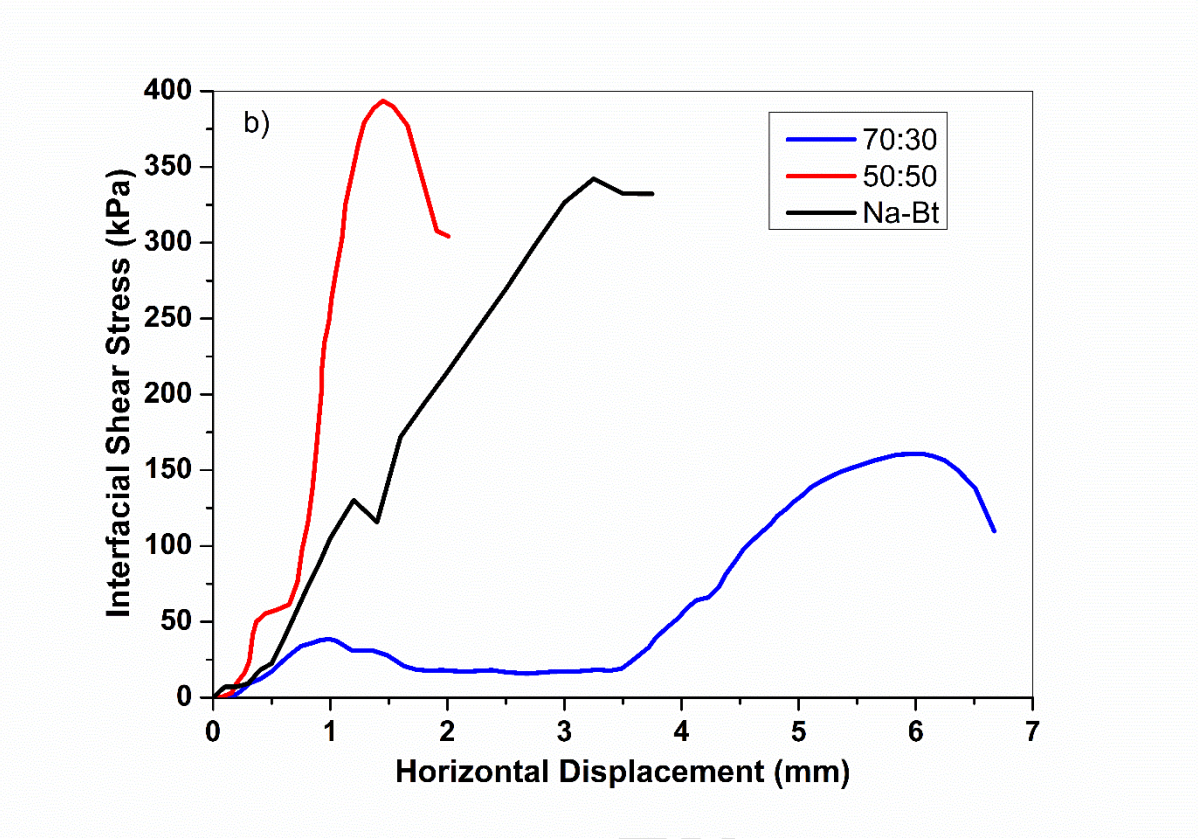

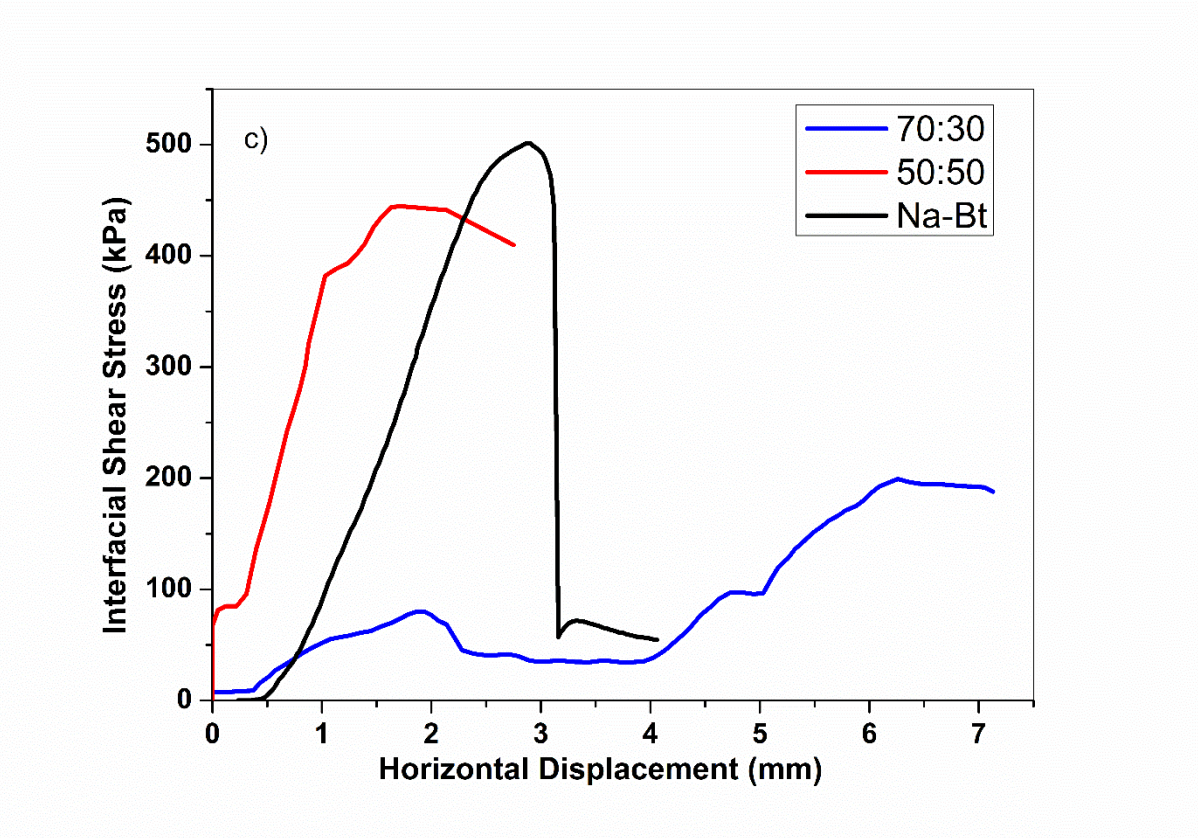

Figure 8. Interfacial adhesive stress versus horizontal displacement obtained for the epoxy coated three soil mixtures under consideration (Na-Bt, 50:50 and 70:30) a) 100 kPa, b) 200 kPa and c) 300 kPa

https://doi.org/10.1180/clm.2024.7 Published online by Cambridge University Press

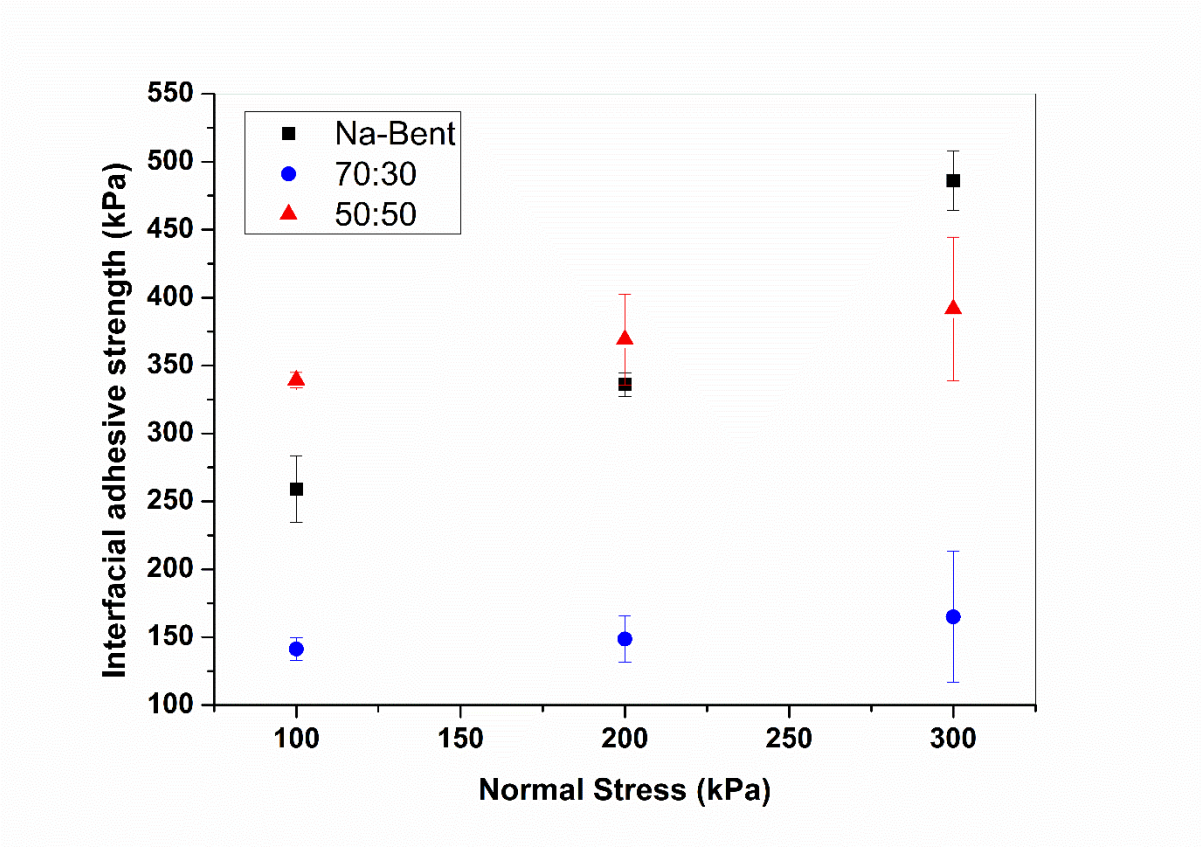

Figure 9 Variation of interfacial adhesive strength with normal stress for all the soils considered. Mixture 50:50 shows highest interfacial adhesive strength at 100 kPa and 200 kPa except at 300 kPa.

The distinct pore microstructure exhibited by clay-sand mixes can be connected to the mechanism by which the individual particles get arranged in the soil. As the clay gets replaced by sand starting from 30% by weight, we can see a clear shift in pore sizes as revealed from NMR measurements. At 30% and 40% of sand fraction, mesopores predominate. This could be due to the gradual formation of sand skeleton from partial to complete state during the static compaction applied to the samples. Compressible behaviour of clay-sand mixtures depends greatly on transition fines content, intergranular void ratio (Cabalar & Hasan, 2013).

https://doi.org/10.1180/clm.2024.7 Published online by Cambridge University Press

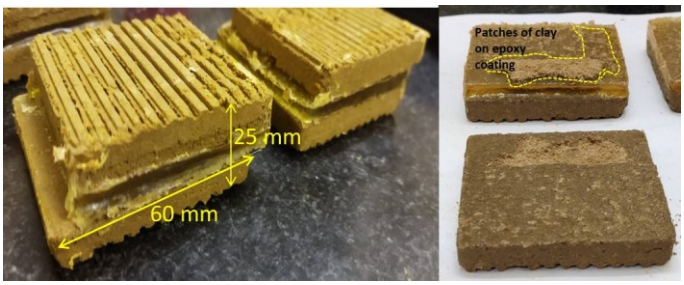

Figure 10 Specimens failed under shear clearly showing adhesive failure at the interface

Thus, clay-sand mixture with a higher macroporosity exhibited the highest interfacial adhesive strength. This is primarily attributed to the thicker diffused interface formation as discussed in our earlier work.

From the findings of differential intrusion curve, the porosity (in the macropore regime) of pure Na-Bt at wet of optimum is found to be similar to clay-sand mixure at 50:50 composition as shown in Figure **12**. However, the interfacial bond strength was significantly different for both of them. Pure Na-Bt at 46.38% water content exhibited a lower interfacial adhesive bond performance at all the normal stresses compared to a 50:50 mixture as shown in the Figure **11**. . Though pure clay is characterised by bimodal distribution, the critical pore radius at macropore region was comparable to clay-sand mixture. Both of these exhibited critical pore entry radius in the macropore regime: 25.38 μm at 0.038 cm^3/g intrusion volume by Na-Bt and 17 μm at 0.022 cm^3/g by 50:50 mix respectively. Even with a higher critical pore entry radius at wet of optimum, the reduction in interfacial performance points to the detrimental effect of moisture content towards interfacial adhesion. As expressed in the critical energy release rate equation, apart from porosity, physical and chemical interactions also have contribution to bond strength. The presence of water might be blocking the access of potential interactive sites for the non-bonded interactions (hydrogen bonds/van der Waal's) and bonded interactions, if any, on the soil substrate. Thus moisture serves as one of the

https://doi.org/10.1180/clm.2024.7 Published online by Cambridge University Press

determining factor for soil porosity and also the interfacial bond strength development with a polymer coating. The effect of porosity due to changes in particle gradation is however reflected at the macro scale interface strength performance.

The macro-mechanical tests conducted on epoxy coated pure clay and various clay-sand mixtures demonstrated the role of porosity towards interface formation. The presence of moisture can be deleterious to interface formation even when a larger pore is available for epoxy penetration. Saturated–surface-dry substrates behaved better than wet surface for interface bonding with a repair material. Importance of surface roughness, moisture state of substrate and viscosity of repair material are elaborated by (Bentz et al., 2018). Also, the negative impact of moisture on interfacial interaction between carbon fibre and epoxy matrix is investigated through molecular dynamics simulation by Tam et al., (2023). The masking of epoxy functional sites and fibre surface by water layer inhibited the molecular scale interactions essential for building up an interface. Similar observations are obtained through this work also, where mechanism behind the lesser bond performance exhibited by epoxy coated on pure Na-Bt having a comparable porosity distribution to a clay-sand mixture is explained.

https://doi.org/10.1180/clm.2024.7 Published online by Cambridge University Press

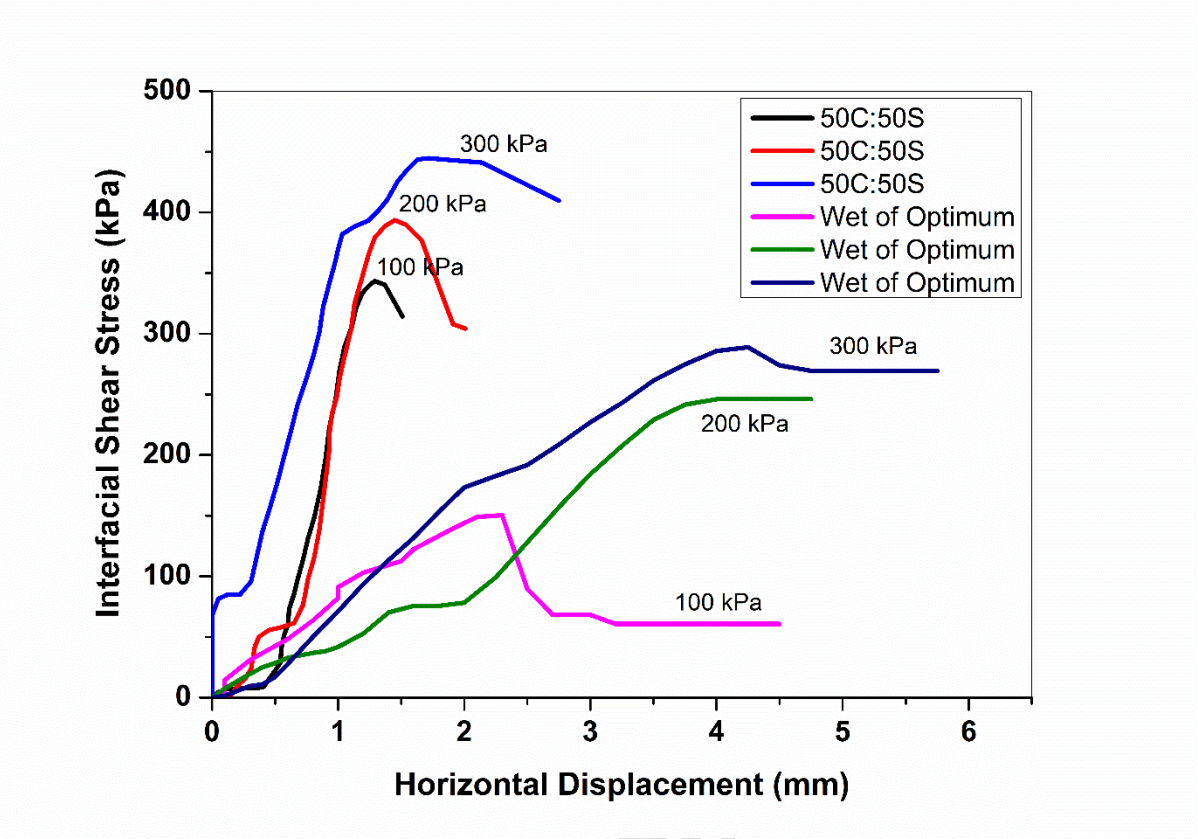

Figure 11 Interfacial adhesive strength exhibited by pure Na-Bt at wet of optimum and 50C:50S at all the normal stresses. Clay-sand mixture exhibited higher strength tha pure clay in all the cases

https://doi.org/10.1180/clm.2024.7 Published online by Cambridge University Press

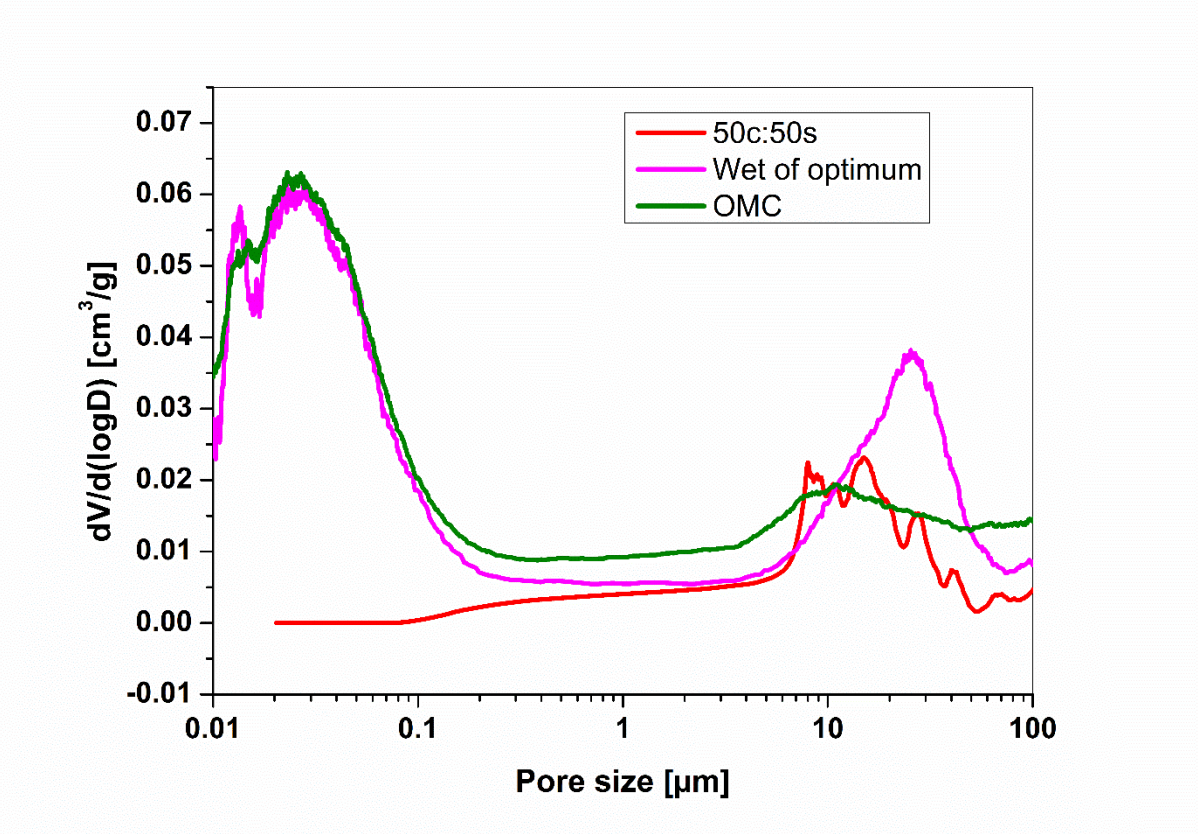

Figure 12 Mercury differential intrusion curves of pure Na-Bt at OMC , wet of optimum and clay-sand at 50:50 proportion

Studies on pore distribution in a marine soft soil with varying clay content shows changes in smallpores (0.02-0.18 µm) and mesopores (≤ 0.18- 0.78 µm) and very low effect on macroporosity (0.78 µm). An increase in clay amount reduced the critical pore entry radius and also reduced the intensity of it referring to the absence of macropores and prominence of nanopores in the soil (Jiao et al., 2021). For clay-sand mixture, we observe an increase in critical pore entry radius with a decrease in clay content. The overall porosity in clay treated with boric acid was around 65% with an average macropore diameter in the range of 2-10 µm

(Kokunešoski et al., 2016). These works are in line with the macropore distribution obtained through this work for pure clay at a higher water content.

4. Conclusions

The interfacial adhesive strength between different clay-sand mixtures and epoxy coating was evaluated in this study. Highest strength was demonstrated by clay-sand mixture of 50:50 composition, thus reflecting the role of porosity towards interfacial strength. Pure clay and clay-sand mixture of 50:50 composition exhibited similar porosity but different interfacial adhesion. This points to the negative impact of moisture on interfacial strength. A deeper understanding of porosity distribution in various clay-sand compositions through MIP and ^{129}Xe NMR was made feasible through this work. A mixture of clay:sand of 50:50 had macroporosity of 74.3 % and mixture of 70:30 had only 3.21 % of macroposity. MIP revealed the exact critical pore entry radius for all the mixtures. The nano-pores, inside clay matrix were evidenced in ^{129}Xe NMR spectra. Though these pore regimes are not beneficial to the interfacial strength development (larger epoxy molecules cannot penetrate to these minute pores), their identification can be helpful in applications involving gaseous particles transport and storage (Luo et al., 2022, Hu et al., 2018) for e.g. methane adsorption or carbon dioxide storage.

CRediT author contribution statement

Nidhi Murali: Conceptualization, Methodology, Formal Analysis, Writing-Original Draft

Jing Li: Methodology (^{129}Xe NMR), Formal Analysis, Writing- Original Draft

Anvi Agarwal: Methodology

Patrick Berthault: Supervision, Methodology

Pijush Ghosh: Supervision, Funding Acquisition

https://doi.org/10.1180/clm.2024.7 Published online by Cambridge University Press

Acknowledgment

The authors would like to acknowledge the financial support from the Science and Engineering Research Board, Government of India for supporting this work (Project No. CRG/2019/003554).

References

Agus, S. S., Schanz, T., & Fredlund, D. G. (2010). Measurements of suction versus water content for bentonite-sand mixtures. *Canadian Geotechnical Journal*, *47*(5), 583–594. https://doi.org/10.1139/T09-120

Alice, A., Donna, D., Ferrari, A., & Laloui, L. (2015). Experimental investigations of the soil-concrete interface : physical mechanisms , cyclic mobilisation and behaviour at different temperatures Swiss Federal Institute of Technology , EPFL , Laboratory for Soil Mechanics EPFL-ENAC-IIC-LMS , Station 18 , CH. *Can. Geotech. J.*, 1–44.

Bentz, D. P., De la Varga, I., Muñoz, J. F., Spragg, R. P., Graybeal, B. A., Hussey, D. S., Jacobson, D. L., Jones, S. Z., & LaManna, J. M. (2018). Influence of substrate moisture state and roughness on interface microstructure and bond strength: Slant shear vs. pull-off testing. *Cement and Concrete Composites*, *87*, 63–72. https://doi.org/https://doi.org/10.1016/j.cemconcomp.2017.12.005

Bonardet, J. L., Fraissard, J., Gédéon, A., & Springuel-Huet, M. A. (1999). Nuclear magnetic resonance of physisorbed 129xe used as a probe to investigate porous solids. *Catalysis Reviews - Science and Engineering*, *41*(2), 115–225. https://doi.org/10.1080/01614949909353779

https://doi.org/10.1180/clm.2024.7 Published online by Cambridge University Press

Briceño, C., Azenha, M., Vasconcelos, G., & Lourenço, P. B. (2024). Influence of conditioning of clay bricks over shear strength of brick masonry. *Journal of Building Engineering*, *82*, 108138. https://doi.org/10.1016/j.jobe.2023.108138

Cabalar, A. F., & Hasan, R. A. (2013). Compressional behaviour of various size/shape sand–clay mixtures with different pore fluids. *Engineering Geology*, *164*, 36–49. https://doi.org/10.1016/j.enggeo.2013.06.011

Carrero-González, B., Carrero-González, B., Cruz, M. T. de la, & Casermeiro, M. Á. (2012). Application of Magnetic Resonance Techniques to evaluate soil compaction after grazing. *Journal of Soil Science and Plant Nutrition*. https://doi.org/10.4067/s0718-95162012000100014

Chen, K., & Liang, F. (2024). Experimental investigation on the dynamic shear behavior of the unsaturated soil-concrete interface under cyclic loading. *Soil Dynamics and Earthquake Engineering*, *176*, 108325. https://doi.org/https://doi.org/10.1016/j.soildyn.2023.108325

Cuthbertson, A. J. S., Samsami, F., & Dong, P. (2018). Model studies for flocculation of sand-clay mixtures. *Coastal Engineering*, *132*, 13–32. https://doi.org/10.1016/j.coastaleng.2017.11.006

Duan, P., Shui, Z., Chen, W., & Shen, C. (2013). Effects of metakaolin, silica fume and slag on pore structure, interfacial transition zone and compressive strength of concrete. *Construction and Building Materials*. https://doi.org/10.1016/j.conbuildmat.2013.02.075

Feng, D., Li, X., Wang, X., Li, J., Sun, F., Sun, Z., Zhang, T., Li, P., Chen, Y., & Zhang, X. (2018). Water adsorption and its impact on the pore structure characteristics of shale clay. *Applied Clay Science*, *155*, 126–138. https://doi.org/10.1016/j.clay.2018.01.017

https://doi.org/10.1180/clm.2024.7 Published online by Cambridge University Press

Filimonova, S., Nossov, A., Dümig, A., Gédéon, A., Kögel-Knabner, I., & Knicker, H. (2011). Evaluating pore structures of soil components with a combination of "conventional" and hyperpolarised 129Xe NMR studies. *Geoderma*, *162*(1), 96–106. https://doi.org/https://doi.org/10.1016/j.geoderma.2011.01.009

Goebel, M.-O., Bachmann, J., Woche, S. K., Fischer, W. R., & Horton, R. (2004). Water Potential and Aggregate Size Effects on Contact Angle and Surface Energy. *Soil Science Society of America Journal*, *68*(2), 383–393. https://doi.org/10.2136/sssaj2004.3830

Gujar, P., Alex, A., Santhanam, M., & Ghosh, P. (2021). Evaluation of interfacial strength between hydrating cement paste and epoxy coating. *Construction and Building Materials*, *279*, 122511. https://doi.org/10.1016/j.conbuildmat.2021.122511

Gujar, P., Murali, N., Ilango, N. K., Santhanam, M., & Ghosh, P. (2023). Engineering interfacial strength of polymer coated hydrating cement paste by tuning calcium characteristics. *Materials and Structures/Materiaux et Constructions*, *56*(3). https://doi.org/10.1617/s11527-023-02154-4

Havens, J. H., & Goodwin., W. A. (1951). *(4) 1. 4*.

Hölck, O., Bauer, J., Wittler, O., Michel, B., & Wunderle, B. (2012). Comparative characterization of chip to epoxy interfaces by molecular modeling and contact angle determination. *Microelectronics Reliability*, *52*(7), 1285–1290. https://doi.org/10.1016/j.microrel.2012.03.019

Horpibulsuk, S., Rachan, R., Chinkulkijniwat, A., Raksachon, Y., & Suddeepong, A. (2010). Analysis of strength development in cement-stabilized silty clay from microstructural considerations. *Construction and Building Materials*, *24*(10), 2011–2021. https://doi.org/10.1016/j.conbuildmat.2010.03.011

https://doi.org/10.1180/clm.2024.7 Published online by Cambridge University Press

Hou, Y., Wang, B., Huang, L., Xu, J., Liu, D., & Jiahua, Z. (2021). Microstructure and Macromechanical Properties of Retaining Structure of Near-Water Reinforced Soil under Dry-Wet Cycle. *Mathematical Problems in Engineering*. https://doi.org/10.1155/2021/6691278

Hu, H., Xing, Y., & Li, X. (2018). Molecular modeling on transportation of CO2 in montmorillonite: Diffusion and permeation. *Applied Clay Science*, *156*, 20–27. https://doi.org/https://doi.org/10.1016/j.clay.2018.01.019

Ilango, N. K., Gujar, P., Nagesh, A. K., Alex, A., & Ghosh, P. (2021). Interfacial adhesion mechanism between organic polymer coating and hydrating cement paste. *Cement and Concrete Composites*, *115*(October 2020), 103856. https://doi.org/10.1016/j.cemconcomp.2020.103856

Jiao, W., Zhou, D., & Wang, Y. (2021). Effects of clay content on pore structure characteristics of marine soft soil. *Water (Switzerland)*, *13*(9), 1–19. https://doi.org/10.3390/w13091160

Khajeh, A., Jamshidi Chenari, R., Payan, M., & MolaAbasi, H. (2023). Assessing the effect of lime-zeolite on geotechnical properties and microstructure of reconstituted clay used as a subgrade soil. *Physics and Chemistry of the Earth, Parts A/B/C*, *132*, 103501. https://doi.org/https://doi.org/10.1016/j.pce.2023.103501

Kokunešoski, M., Šaponjić, A., Stanković, M., Majstorović, J., Egelja, A., Ilić, S., & Matović, B. (2016). Effect of boric acid on the porosity of clay and diatomite monoliths. *Ceramics International*, *42*(5), 6383–6390. https://doi.org/10.1016/j.ceramint.2016.01.034

Li, J., Mailhiot, S., Sreenivasan, H., Kantola, A. M., Telkki, V.-V., & Kinnunen, P. (2022).

https://doi.org/10.1180/clm.2024.7 Published online by Cambridge University Press

129Xe NMR analysis reveals efficient gas transport between inborn micro-, meso- and macropores in geopolymers. *Cement and Concrete Research*, *155*, 106779. https://doi.org/https://doi.org/10.1016/j.cemconres.2022.106779

Lubelli, B., de Winter, D. A. M., Post, J. A., van Hees, R. P. J., & Drury, M. R. (2013). Cryo-FIB-SEM and MIP study of porosity and pore size distribution of bentonite and kaolin at different moisture contents. *Applied Clay Science*, *80–81*, 358–365. https://doi.org/10.1016/j.clay.2013.06.032

Luo, Q., Li, Y., Zhang, Z., Peng, X., & Geng, G. (2022). Influence of substrate moisture on the interfacial bonding between calcium silicate hydrate and epoxy. *Construction and Building Materials*, *320*. https://doi.org/10.1016/j.conbuildmat.2021.126252

Miller, E. A., & Sowers, G. . (1958). The strength characteristics of soil-aggregate mixtures & discussion. *Highway Research Board Bulletin*, *183*, 16–32.

Murali, N., Gujar, P., & Ghosh, P. (2022). Performance of clay–epoxy interface at different points on proctor curve. *Applied Clay Science*, *226*(December 2021), 106553. https://doi.org/10.1016/j.clay.2022.106553

Orts, W. J., Roa-Espinosa, A., Sojka, R. E., Glenn, G. M., Imam, S. H., Erlacher, K., & Pedersen, J. S. (2007). Use of Synthetic Polymers and Biopolymers for Soil Stabilization in Agricultural, Construction, and Military Applications. *Journal of Materials in Civil Engineering*, *19*(1), 58–66. https://doi.org/10.1061/(asce)0899-1561(2007)19:1(58)

Pan, J., Wang, B., Wang, Q., Ling, X., Fang, R., Liu, J., & Wang, Z. (2023). Thickness of the shear band of silty clay–concrete interface based on the particle image velocimetry technique. *Construction and Building Materials*, *388*. https://doi.org/10.1016/j.conbuildmat.2023.131712

https://doi.org/10.1180/clm.2024.7 Published online by Cambridge University Press

Shafizadeh, A., Gimmi, T., Van Loon, L. R., Kaestner, A. P., Mäder, U. K., & Churakov, S. V. (2020). Time-resolved porosity changes at cement-clay interfaces derived from neutron imaging. *Cement and Concrete Research*, *127*, 105924. https://doi.org/https://doi.org/10.1016/j.cemconres.2019.105924

Soltani-Jigheh, H., Bagheri, M., & Amani-Ghadim, A. R. (2019). Use of hydrophilic polymeric stabilizer to improve strength and durability of fine-grained soils. *Cold Regions Science and Technology*, *157*(October 2018), 187–195. https://doi.org/10.1016/j.coldregions.2018.10.011

Tam, L., Ntjam Minkeng, M. A., Lau, D., Mansour, W., & Wu, C. (2023). Molecular interfacial shearing creep behavior of carbon fiber/epoxy matrix interface under moisture condition. *Engineering Fracture Mechanics*, *282*, 109177. https://doi.org/https://doi.org/10.1016/j.engfracmech.2023.109177

Tripathi, K. K., & Viswanadham, B. V. S. (2012). Evaluation of the Permeability Behaviour of Sand-Bentonite Mixtures Through Laboratory Tests. *Indian Geotechnical Journal*, *42*(4), 267 – 277. https://doi.org/10.1007/s40098-012-0020-8

Tsiao, C.-J., Carrado, K. A., & Botto, R. E. (1998). Investigation of the microporous structure of clays and pillared clays by 129Xe NMR. *Microporous and Mesoporous Materials*, *21*(1), 45–51. https://doi.org/https://doi.org/10.1016/S1387-1811(97)00040-1

Wang, Y. B., Zhao, C., & Wu, Y. (2020). Study on the effects of grouting and roughness on the shear behavior of cohesive soil-concrete interfaces. *Materials*, *13*(14). https://doi.org/10.3390/ma13143043

Watabe, Y., Yamada, K., & Saitoh, K. (2011). Hydraulic conductivity and compressibility of mixtures of Nagoya clay With Sand Or Bbntonite. *Geotechnique*, *61*(3), 211 – 219.

https://doi.org/10.1180/clm.2024.7 Published online by Cambridge University Press

https://doi.org/10.1680/geot.8.P.087

Wu, Y., Zhang, X., Zhao, C., & Zhao, C. (2023). Effects of soil unloading and grouting on the vertical bearing mechanism for compressive piles. *Ocean Engineering*, *271*, 113754. https://doi.org/https://doi.org/10.1016/j.oceaneng.2023.113754

Xia, W., Wang, Q., Yu, Q., Yao, M., Sun, D., Liu, J., & Wang, Z. (2023). Experimental investigation of the mechanical properties of hydrophobic polymer-modified soil subjected to freeze–thaw cycles. *Acta Geotechnica*, *18*(7), 3623–3642. https://doi.org/10.1007/s11440-023-01804-9

Zhu, H., Li, S., Hu, Z., Ju, Y., Pan, Y., Yang, M., Lu, Y., Wei, M., & Qian, W. (2023). Microstructural observations of clay-hosted pores in black shales: implications for porosity preservation and petrophysical variability. *Clay Minerals*, *58*(3), 310–323. https://doi.org/10.1180/clm.2023.28

https://doi.org/10.1180/clm.2024.7 Published online by Cambridge University Press